Alternative LISA-TAIJI networks

Gang Wang,[1,*] Wei-Tou Ni,[2,3,†] Wen-Biao Han,[1,4,5,‡] Peng Xu,[6,7,4,§] and Ziren Luo[4,6,8,‖]

[1]*Shanghai Astronomical Observatory, Chinese Academy of Sciences, Shanghai 200030, China*
[2]*State Key Laboratory of Magnetic Resonance and Atomic and Molecular Physics, Innovation Academy for Precision Measurement Science and Technology (APM), Chinese Academy of Sciences, Wuhan 430071, China*
[3]*Department of Physics, National Tsing Hua University, Hsinchu, Taiwan, 30013, Republic of China*
[4]*Hangzhou Institute for Advanced Study, University of Chinese Academy of Sciences, Hangzhou 310124, China*
[5]*School of Astronomy and Space Science, University of Chinese Academy of Sciences, Beijing 100049, China*
[6]*Institute of Mechanics, Chinese Academy of Sciences, Beijing 100190, China*
[7]*Lanzhou Center for Theoretical Physics, Lanzhou University, Lanzhou 730000, China*
[8]*Taiji Laboratory for Gravitational Wave Universe (Beijing/Hangzhou), University of Chinese Academy of Sciences, Beijing 100049, China*

(Received 11 May 2021; accepted 4 June 2021; published 6 July 2021)

The spaceborne gravitational wave (GW) detectors LISA and TAIJI are planned to be launched in the 2030s. The dual detectors with comparable sensitivities will form a network observing GWs with significant advantages. In this work, we investigate the three possible LISA-TAIJI networks for the different location and orientation compositions of the LISA orbit (+60° inclination and trailing the Earth by 20°) and alternative TAIJI orbit configurations, including TAIJIp (+60° inclination and leading the Earth by 20°), TAIJIc (+60° inclination and colocated with LISA), and TAIJIm (−60° inclination and leading the Earth by 20°). Of the three LISA-TAIJI configurations, the LISA-TAIJIm network shows the best performance in the sky localization and polarization determination for massive binary systems due to its better complementary antenna pattern, and LISA-TAIJIc could achieve the best cross-correlation and observe the stochastic GW background with optimal sensitivity.

DOI: 10.1103/PhysRevD.104.024012

I. INTRODUCTION

The gravitational wave (GW) detection GW150914 was observed by Advanced LIGO detectors at two sites: Hanford, WA, and Livingston, LA [1]. These two interferometers are designed to be (closely) aligned interferometric arms with a separation of 3000 km. GW170814 and GW170817 were the first detections coincidently observed by the triple interferometers of Advanced LIGO and Advanced Virgo. As benefits of the misaligned orientation between the LIGO and Virgo detectors, the source directions were well localized, and alternative GW polarizations were tested [2–4]. The KAGRA detector is expected to join the ground-based interferometer network in the near future [5,6]. The detector network surrounding the Earth will improve the angular resolution of the sky localization and parameter determination on the GW sources [6,7]. Although the current GW detections are all from compact binary coalescences, Advanced LIGO and Advanced Virgo are actively searching for the stochastic GW background (SGWB) [8–13]. Detection of the stochastic relic GWs will deeply impact our understanding of the early Universe. To distinguish the cosmological imprint from instrument noise and the astrophysical foreground, joint observations from two or more independent detectors are highly demanded.

Multiple interferometer cooperation is also planned in the next-generation space missions for GW observation in the deci-Hz middle frequency band. Both the BBO and DECIGO missions proposed three constellations deployed on an Earth-like heliocentric orbit with 120° separations [14,15]. The number of detectors will increase the signal-to-noise ratio (SNR) of the detection, and the large separations between the constellations will improve the angular resolution of the sky localization for the sources. The SGWB is also expected to be observed by the two colocated and coplanar interferometers of BBO or DECIGO [16,17]. The present activities of GW missions in this middle frequency band are briefly reviewed in Ref. [18].

*gwang@shao.ac.cn, gwanggw@gmail.com
†weitou@gmail.com
‡wbhan@shao.ac.cn
§xp@lzu.edu.cn
‖luoziren@imech.ac.cn

The spaceborne missions targeting milli-Hz low-frequency-band GW observations, including LISA [19], TAIJI [20], and TianQin [21], are scheduled to be launched around the 2030s. Each of the missions will include a triangular constellation formed by three spacecraft. The LISA and TAIJI missions are designed to use a heliocentric orbit. To achieve stable interferometer arms, the spacecraft formation plane of LISA/TAIJI is designed to be $\pm 60°$ with the ecliptic by employing the Clohessy-Wiltshire framework [22]. By assuming that TAIJI is leading the Earth by 20° and LISA is trailing the Earth by 20°, Ruan *et al.* [23] and Wang *et al.* [24] investigated the sky localization improvement of the LISA-TAIJI network compared to the LISA mission alone. Omiya and Seto [25], Seto [26], and Orlando *et al.* [27] evaluated network capabilities for the SGWB observation. Wang *et al.* [28] and Wang *et al.* [29] estimated the impact of the joint LISA-TAIJI observation on cosmological parameter determination. Wang and Han [30] demonstrated the observation constraints on the GW polarizations from the joint observation.

Considering that the orbital configuration of the TAIJI mission is not fully determined, the merits of the alternative LISA-TAIJI networks are worth evaluating. In this work, by presetting the LISA orbit as determined, we investigate the performances of three possible LISA-TAIJI networks for different TAIJI orbital selections, as shown in Fig. 1:

(a) TAIJIp, which leads the Earth by ∼20°, with the formation of the constellation at a +60° inclination, as with LISA.
(b) TAIJIm, which also leads the Earth by ∼20°, with the plane of the spacecraft at a −60° inclination, in contrast to LISA.
(c) TAIJIc, which is colocated and coplanar with LISA, trailing the Earth by ∼20°.

The deployment and observation for the TAIJI mission from these orbit choices are expected to be not much different. However, joint observations with LISA from alternative TAIJI mission orbits could yield different performances for supermassive black hole (SMBH) binary and SGWB observations. We evaluate networks' angular resolutions of sky localization for SMBH binary, amplitude determination for alternative polarizations beyond general relativity (GR), and the overlap reduction function for the SGWB observations. In the three pair combinations, the LISA-TAIJIm network demonstrates the best parameter determinations for SMBH binary systems, and LISA-TAIJIc shows an optimal capability for the SGWB observation.

This paper is organized as follows: In Sec. II, we introduce three LISA-TAIJI network configurations and their joint sensitivities. In Sec. III, we report and compare the results of parameter determinations on SMBH binaries from the three LISA-TAIJI networks, including the angular resolution and the alternative polarization constraints. In Sec. IV, we investigate the overlap reduction functions of the three networks for the SGWB observation. We recapitulate our conclusions in Sec. V. (We set $G = c = 1$ in this work except where otherwise stated.)

II. ALTERNATIVE LISA-TAIJI NETWORKS

A. The LISA and TAIJI orbital configurations

The LISA mission, scheduled to be launched in the 2030s, includes three spacecraft forming a 2.5×10^6 km triangle trailing the Earth by 20° [19]. The constellation plane has a 60° inclination with respect to the ecliptic plane, as shown in Fig. 1. The TAIJI mission is proposed as a LISA-like orbital configuration with a 3×10^6 km arm length [20]. An assumed orbit for the TAIJI spacecraft has the constellation in front of the Earth by 20° and has the same 60° inclination as LISA, as shown in the left plot of Fig. 1, and this TAIJI orbital configuration is labeled as TAIJIp in this work. The preset 20° trailing/leading angle is a practical compromise from the launch vehicle, telemetry capabilities, and the gravitational perturbation reduction [31].

The TAIJI orbital configuration could also have other choices without (significantly) increasing the launch budget. The first alternative is for the constellation formation to be tuned to a −60° inclination (rather than TAIJIp's +60°), and we label this configuration TAIJIm.

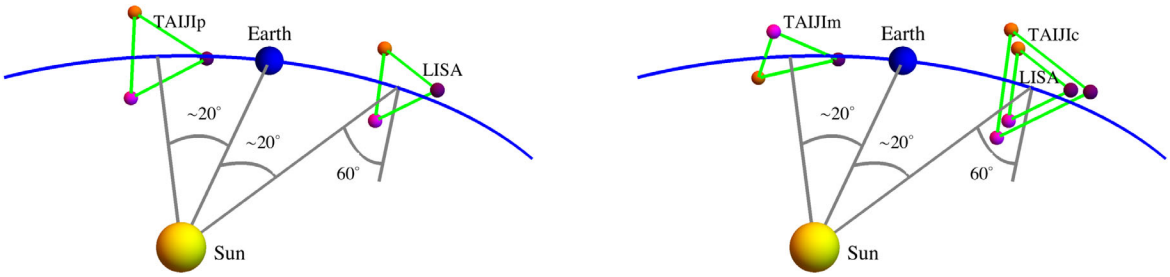

FIG. 1. Diagrams of LISA and TAIJI mission orbital configurations. The left panel shows LISA (trailing the Earth by ∼20° and +60° inclined with respect to the ecliptic plane) and TAIJIp (leading the Earth by ∼20° and +60° inclined). The right panel shows LISA and two other optional TAIJI orbital choices: TAIJIm (leading the Earth by ∼20° and with a −60° inclination) and TAIJIc (coplanar and colocated with LISA). The angle between the LISA and TAIJIp formation planes is ∼34.5°, and the angle between the LISA and TAIJIm formation planes is ∼71°.

Another alternative is for TAIJI to be colocated and coplanar with LISA, which we label as TAIJIc in this work. These two orbital configurations are shown in the right panel of Fig. 1. For the LISA-TAIJIc network, the orientations of the two spacecraft formations would be coaligned. For LISA-TAIJIp, the angle between the two formation planes is ∼34.5°, their separation angle is ∼40°, and their distance is $\sim 1 \times 10^8$ km. The angle of the orientations between LISA and TAIJIm is around 71°.

In this work, by employing numerical orbits, we investigate the performances of three pairs of LISA-TAIJI network configurations (LISA-TAIJIp, LISA-TAIJIm, and LISA-TAIJIc) regarding detectability for SMBH binaries and the SGWB. These three combinations should cover all the possible dual detector scenarios except for LISA with a colocated TAIJI having a −60° inclination, which would be insipid, because it would benefit from-cover neither a large separation for the compact binary observations nor strong cross-correlation for SGWB observation. The numerical orbits for the TAIJIp and TAIJIc are from our work in Refs. [24,32], and the orbit for TAIJIm iscover newly obtained from our optimization method in Refs. [32–37].

B. Response formulation of TDI channel

For the spaceborne GW missions, time-delay interferometry (TDI) is essential to suppress the laser frequency noise and achieve targeting sensitivity. The sensitivities for the different TDI channels have been evaluated numerically in our recent works [38,39]. When implementing TDI, the GW response is combined from the response of each evolved single link. The response functions to the GW tensor polarizations from GR in Doppler measurements were formulated in Refs. [40–43], and the response functions to the polarizations beyond the GR were developed by Tinto and da Silva Alves [44]. To keep the integrity of the work, we reiterate the formulas of the response of TDI to the six polarizations as utilized in Ref. [30].

The GW propagation vector from a source located at ecliptic longitude λ and latitude θ (in the Solar System barycentric coordinates) will be

$$\hat{k} = -(\cos\lambda\cos\theta, \sin\lambda\cos\theta, \sin\theta). \tag{1}$$

The polarization tensors of the GW signal for the +, ×, scalar breathing (b), scalar longitudinal (L), and vectors x and y, combining with the factors of the source's inclination angle ι, are

$$\begin{aligned}
&e_+ \equiv \mathcal{O}_1 \cdot \begin{pmatrix} 1 & 0 & 0 \\ 0 & -1 & 0 \\ 0 & 0 & 0 \end{pmatrix} \cdot \mathcal{O}_1^T \times \frac{1+\cos^2\iota}{2}, \qquad e_\times \equiv \mathcal{O}_1 \cdot \begin{pmatrix} 0 & 1 & 0 \\ 1 & 0 & 0 \\ 0 & 0 & 0 \end{pmatrix} \cdot \mathcal{O}_1^T \times i(-\cos\iota), \\
&e_b \equiv \mathcal{O}_1 \cdot \begin{pmatrix} 1 & 0 & 0 \\ 0 & 1 & 0 \\ 0 & 0 & 0 \end{pmatrix} \cdot \mathcal{O}_1^T \times \sin^2\iota, \qquad e_L \equiv \mathcal{O}_1 \cdot \begin{pmatrix} 0 & 0 & 0 \\ 0 & 0 & 0 \\ 0 & 0 & 1 \end{pmatrix} \cdot \mathcal{O}_1^T \times \sin^2\iota, \\
&e_x \equiv \mathcal{O}_1 \cdot \begin{pmatrix} 0 & 0 & 1 \\ 0 & 0 & 0 \\ 1 & 0 & 0 \end{pmatrix} \cdot \mathcal{O}_1^T \times \sin\iota\cos\iota, \qquad e_y \equiv \mathcal{O}_1 \cdot \begin{pmatrix} 0 & 0 & 0 \\ 0 & 0 & 1 \\ 0 & 1 & 0 \end{pmatrix} \cdot \mathcal{O}_1^T \times i\sin\iota,
\end{aligned} \tag{2}$$

with

$$\mathcal{O}_1 = \begin{pmatrix} \sin\lambda\cos\psi - \cos\lambda\sin\theta\sin\psi & -\sin\lambda\sin\psi - \cos\lambda\sin\theta\cos\psi & -\cos\lambda\cos\theta \\ -\cos\lambda\cos\psi - \sin\lambda\sin\theta\sin\psi & \cos\lambda\sin\psi - \sin\lambda\sin\theta\cos\psi & -\sin\lambda\cos\theta \\ \cos\theta\sin\psi & \cos\theta\cos\psi & -\sin\theta \end{pmatrix}, \tag{3}$$

where ψ is the polarization angle. The response to the GW polarization "p" in the link from spacecraft i to spacecraft j will be

$$y^h_{p,ij}(f) = \frac{\hat{n}_{ij} \cdot e_p \cdot \hat{n}_{ij}}{2(1 - \hat{n}_{ij} \cdot \hat{k})} \times [\exp(2\pi i f(L_{ij} + \hat{k} \cdot p_i)) - \exp(2\pi i f \hat{k} \cdot p_j)], \tag{4}$$

where $\hat{n}_{ij}$ is the unit vector from spacecraft i to j, L_{ij} is the arm length from spacecraft i to j, and p_i is the position of spacecraft i in the Solar System barycentric ecliptic coordinates.

The first-generation Michelson TDI configuration and its corresponding optimal channels are employed to represent the performance of each mission. The response of the Michelson-X channel for a specific polarization "p" in the

frequency domain will be the sum of the responses in the time-shift single links,

$$\begin{aligned} F_{\mathrm{X,p}}(f) = &(-\Delta_{21} + \Delta_{21}\Delta_{13}\Delta_{31}) y^h_{\mathrm{p},12} \\ &+ (-1 + \Delta_{13}\Delta_{31}) y^h_{\mathrm{p},21} \\ &+ (\Delta_{31} - \Delta_{31}\Delta_{12}\Delta_{21}) y^h_{\mathrm{p},13} \\ &+ (1 - \Delta_{12}\Delta_{21}) y^h_{\mathrm{p},31}, \end{aligned} \tag{5}$$

where $\Delta_{ij} = \exp(2\pi i f L_{ij})$. The GW responses in the Michelson optimal A, E, and T channels are obtained by applying [42,45]

$$\mathrm{A} = \frac{\mathrm{Z}-\mathrm{X}}{\sqrt{2}}, \quad \mathrm{E} = \frac{\mathrm{X}-2\mathrm{Y}+\mathrm{Z}}{\sqrt{6}}, \quad \mathrm{T} = \frac{\mathrm{X}+\mathrm{Y}+\mathrm{Z}}{\sqrt{3}}, \tag{6}$$

where the Y and Z channels are obtained from cyclical permutation of the spacecraft indices in the X channel.

C. The sensitivity of the networks

1. The noises in TDI

Multiple noise sources will be involved in the process of TDI combinations from the link measurements. For the Michelson-X channels, the expression of measurements could be described as [43]

$$\begin{aligned} \mathrm{X} = &[\mathcal{D}_{31}\mathcal{D}_{13}\mathcal{D}_{21}\eta_{12} + \mathcal{D}_{31}\mathcal{D}_{13}\eta_{21} + \mathcal{D}_{31}\eta_{13} + \eta_{31}] \\ &- [\eta_{21} + \mathcal{D}_{21}\eta_{12} + \mathcal{D}_{21}\mathcal{D}_{12}\eta_{31} + \mathcal{D}_{21}\mathcal{D}_{12}\mathcal{D}_{31}\eta_{13}], \end{aligned} \tag{7}$$

where $\mathcal{D}_{ij}$ is a time-delay operator, $\mathcal{D}_{ij}\eta(t) = \eta(t - L_{ij})$, η_{ji} are the combined observables from spacecraft j to spacecraft i [46–48], and the specific expressions for this work are defined in Ref. [39]. By assuming the dominant laser frequency noises are sufficiently suppressed, the acceleration noise and optical path noise in η_{ij} become the primary noise sources after the TDI process.

The noise budgets for the acceleration noise S_{acc} are assumed to be the same for LISA and TAIJI [19,49]:

$$S^{1/2}_{\mathrm{acc}} = 3\times10^{-15}\,\frac{\mathrm{m/s^2}}{\sqrt{\mathrm{Hz}}}\sqrt{1+\left(\frac{0.4\,\mathrm{mHz}}{f}\right)^2}\sqrt{1+\left(\frac{f}{8\,\mathrm{mHz}}\right)^4}. \tag{8}$$

The optical path noise requirements S_{op} for the two missions are treated slightly differently, as

$$S^{1/2}_{\mathrm{op,LISA}} = 10\times10^{-12}\,\frac{\mathrm{m}}{\sqrt{\mathrm{Hz}}}\sqrt{1+\left(\frac{2\ \mathrm{mHz}}{f}\right)^4}, \tag{9}$$

$$S^{1/2}_{\mathrm{op,TAIJI}} = 8\times10^{-12}\,\frac{\mathrm{m}}{\sqrt{\mathrm{Hz}}}\sqrt{1+\left(\frac{2\ \mathrm{mHz}}{f}\right)^4}. \tag{10}$$

The power spectrum density (PSD) of a TDI channel $\mathrm{S}_{n,\mathrm{TDI}}$ is obtained by implementing the numerical algorithm developed in Refs. [38,39].

2. The joint sensitivities

The antenna pattern of an interferometer will change with the geometric angles $\Omega(\lambda,\theta,\psi,\iota)$ and the frequency. For a given Ω and frequency, the sensitivities of LISA's A + E + T channel and the joint LISA-TAIJI network at a given mission time could be evaluated, respectively, by

$$\begin{aligned} \mathrm{S}^{1/2}_{\mathrm{LISA}}(f,\Omega) &= \left(\sum_{\mathrm{A,E,T}} \frac{|F_{\mathrm{TDI}}(f,\Omega)|^2}{\mathrm{S}_{n,\mathrm{TDI}}(f)}\right)^{-1/2}, \\ \mathrm{S}^{1/2}_{\mathrm{joint}}(f,\Omega) &= \left(\sum_{\mathrm{LISA}}^{\mathrm{TAIJI}} \sum_{\mathrm{A,E,T}} \frac{|F_{\mathrm{TDI}}(f,\Omega)|^2}{\mathrm{S}_{n,\mathrm{TDI}}(f)}\right)^{-1/2}. \end{aligned} \tag{11}$$

The instantaneous sensitivities to the tensor polarizations for the LISA and joint LISA-TAIJI networks for $\psi = 0$, $\iota = 0$, and $f = 10$ mHz are shown in Fig. 2. As we can see in the upper-left plot, LISA has its optimum sensitivity around the normal directions (ecliptic latitude $\pm30°$) of the triangular formation plane considering its 60° inclination. As expected from Fig. 1, the antenna pattern of the TAIJIp configuration is shifted by ∼40° along the ecliptic latitude with respect to LISA's, and their joint sensitivity is shown by the upper-right panel in Fig. 2. For the TAIJIm network, due to its 40° separation and −60° inclination with respect to LISA, its antenna pattern is not only shifted by 40° along the latitude, but also inverted with respect to the ecliptic plane, and the joint sensitivity of the LISA-TAIJIm configuration is shown in the lower-left panel. As for the TAIJIc case, since the TAIJIc is colocated and coplanar with LISA, the joint LISA-TAIJIc configuration enhances LISA's sensitivity, as shown in the lower-right plot. One caveat is that the sensitivity of the TAIJI is slightly better than that of the LISA mission; full symmetry should not be expected for the joint sensitivity plots in Fig. 2.

III. PARAMETER DETERMINATIONS FOR SMBH BINARY COALESCENCE

As the most promising GW source for the LISA and TAIJI missions, the SMBH binary is selected to demonstrate the performances of parameter determination from LISA and the three LISA-TAIJI networks.

A. Fisher information method

The Fisher information matrix (FIM) is employed in this investigation to determine the uncertainty of parameters

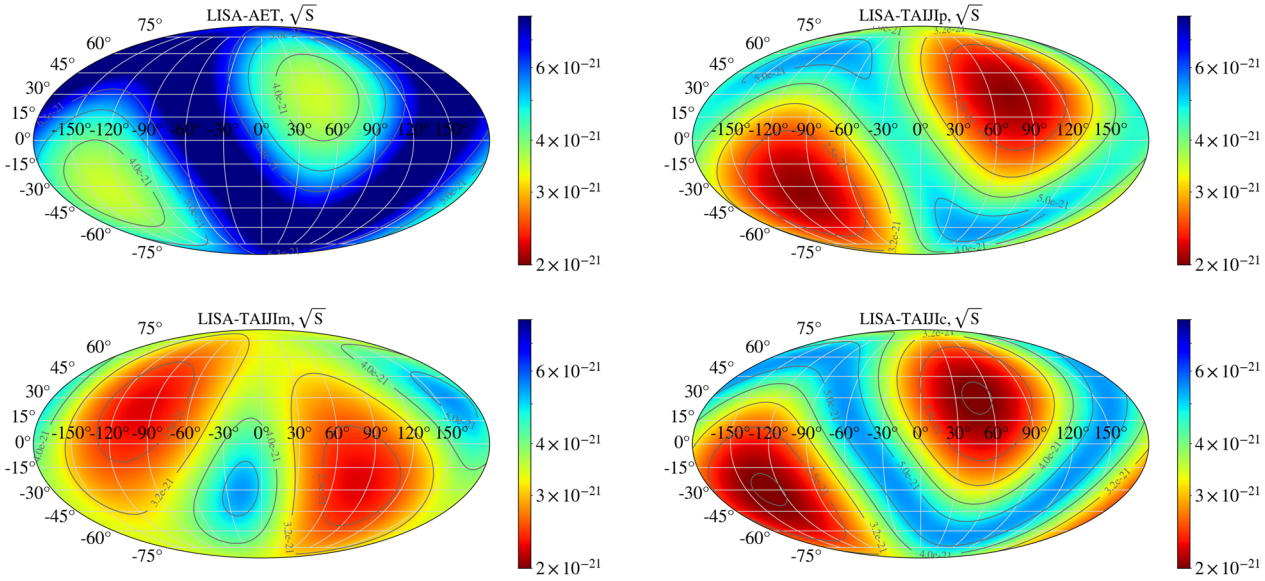

FIG. 2. The instantaneous sensitivities on the sky map for the LISA mission and LISA-TAIJI networks at $\psi = 0$, $\iota = 0$, and $f = 10$ mHz. LISA's sensitivity alone is shown by the upper-left panel, which is obtained using Eq. (10), and the joint LISA-TAIJI network sensitivities are obtained by using Eq. (11). The sensitivity of the LISA-TAIJIp configuration is shown in the upper-right panel, the sensitivity of LISA-TAIJIm is shown in the lower-left panel, and the sensitivity of LISA-TAIJIc is shown in the lower-right panel. The plots reflect the antenna pattern of the detectors, considering the orientation of the spacecraft formations. The LISA-TAIJIm network achieves a better averaged sensitivity to the different sky directions than the other two networks. (One caveat is that the sensitivity of the TAIJI is slightly better than that of the LISA mission; full symmetry on the plots should not be expected.)

from GW observation (see Refs. [50–53] and references therein). For a single mission with a full six links, the FIM is combined from three optimal channels (A, E, and T), and the FIM of the joint LISA-TAIJI network is obtained by summing up the FIMs from two missions:

$$\Gamma_{ij} = \sum_{\text{LISA}}^{\text{TAIJI}} \sum_{\text{A,E,T}} \left(\frac{\partial \tilde{h}_{\text{TDI}}}{\partial \xi_i} \middle| \frac{\partial \tilde{h}_{\text{TDI}}}{\partial \xi_j} \right) \tag{12}$$

and

$$(g|h)_{\text{TDI}} = 4\text{Re} \int_0^\infty \frac{g^*(f)h(f)}{S_{\text{TDI}}(f)} \mathrm{d}f, \tag{13}$$

where $\tilde{h}_{\text{TDI}}$ is the frequency-domain GW waveform responding in a TDI channel, ξ_i is the ith parameter to be determined, and $S_{\text{TDI}}(f)$ is the noise PSD of the corresponding TDI channel.

Considering that the source location estimation will be significantly affected by the polarization content of the source [2–4], only tensor polarizations from GR are included to investigate the angular resolution of the sky localization. Nine parameters are utilized to describe the GW signal and TDI responses from the LISA or LISA-TAIJI network: ecliptic longitude and latitude (λ, θ), polarization angle ψ, source inclination ι, luminosity distance D, the coalescence time and phase (t_c, ϕ_c), the total mass of the binary M, and the mass ratio q. The GW signal response from TDI incorporating two polarizations ($+$ and $\times$) could be described as

$$\tilde{h}_{\text{GR,TDI}}(f) = (F_+ + F_\times)\tilde{h}_{\text{GR}}, \tag{14}$$

where $\tilde{h}_{\text{GR}}$ is the frequency-domain waveform represented by IMRPhenomPv2 [54]. When the constraints on the alternative GW polarizations are investigated, six additional ppE (parametrized post-Einsteinian) parameters $(\beta, b, \alpha_{\text{b}}, \alpha_{\text{L}}, \alpha_{\text{x}}, \alpha_{\text{x}})$ are employed to qualify the deviations from the GR as developed in Ref. [55], and the waveform will be explained in Eq. (18).

The variance-covariance matrix of the parameters is calculated by

$$\langle \Delta\xi_i \Delta\xi_j \rangle = (\Gamma^{-1})_{ij} + \mathcal{O}(\rho^{-1}) \overset{\rho \gg 1}{\simeq} (\Gamma^{-1})_{ij}. \tag{15}$$

The standard deviations σ_i and correlation σ_{ij} of the parameters for the high SNR $\rho \gg 1$ will be

$$\begin{aligned} \sigma_i &\simeq \sqrt{(\Gamma^{-1})_{ii}}, \\ \sigma_{ij} &= \text{cov}(\xi_i, \xi_j) \simeq (\Gamma^{-1})_{ij}. \end{aligned} \tag{16}$$

The uncertainty of the sky localization for one source is evaluated by

$$\Delta\Omega \simeq 2\pi|\cos\theta|\sqrt{\sigma_\lambda\sigma_\theta - \sigma_{\lambda\theta}^2}. \quad (17)$$

The Monte Carlo simulation is performed for parameter determination by 1000 sources. The (λ, θ) values are randomly sampled in the sky sphere, ψ is sampled in $[0, 2\pi]$ uniformly, $\cos\iota$ is sampled randomly in $[-1, 1]$, and the merge time t_c is sampled randomly for one year. The values $m_1 = 10^5\ M_\odot$ and $q = 1/3$ at redshift $z = 2$ are fixed as used in Refs. [24,30]. Considering that the SNR is mainly contributed from the binary coalescing stage, a 30 day observation before the merge is simulated to perform the investigation.

B. Sky localization of the networks

The cumulative histograms of the SNR from the LISA and LISA-TAIJI networks are shown in the left panel of Fig. 3. Compared to the single LISA mission, all three LISA-TAIJI networks achieve more than $\sqrt{2}$ times the SNR by implementing the quadratic sum ($\rho^2_{\rm joint} = \rho^2_{\rm LISA} + \rho^2_{\rm TAIJI}$), considering that TAIJI is more sensitive than LISA in the selected GW frequency band. Of the three networks, the LISA-TAIJIc has a larger range of SNR distribution with a longer tail, because the coaligned detectors are sensitive/insensitive to the same directions and leave common optimal/blind areas. The LISA-TAIJIm network shows the most concentrated SNR values compared to the two other networks, since its joint antenna pattern is more averaged on the sky map, as shown in Fig. 2.

The angular resolutions of the sky localization from the LISA and LISA-TAIJI networks are shown in the right panel of Fig. 3. For the LISA-TAIJIc network, the uncertainties of sky localization are improved by more than a factor of 2 compared to the single LISA mission, which should be due to the more than $\sqrt{2}$ times SNR from the network. Compared to the LISA-TAIJIc, the joint observation from the LISA-TAIJIp configuration demonstrates an improvement of over 2 orders of magnitude on the localization resolution, which should be mainly attributed to the long baseline separations between LISA and TAIJIp. On the other side, the LISA-TAIJIm network yields a better capability of locating the source than LISA-TAIJIp because the TAIJIm's formation plane is 71° with respect to LISA's, and its antenna pattern can better compensate for LISA's insensitive directions.

C. Observation for GW polarizations

The detector's GW signal response is modified as follows to incorporate alternative polarization beyond GR [30,55]:

$$\begin{aligned}\tilde{h}_{\rm ppE,TDI}(f) = [&(F_{\rm TDI,+} + F_{\rm TDI,\times})(1 + C\beta u_2^{b+5}) \\ &+\alpha_{\rm b}F_{\rm TDI,b} + \alpha_{\rm L}F_{\rm TDI,L} \\ &+\alpha_{\rm x}F_{\rm TDI,x} + \alpha_{\rm y}F_{\rm TDI,y}]\tilde{h}_{\rm GR}e^{2i\beta u_2^b},\end{aligned} \quad (18)$$

where C is a function of b defined by Eq. (11) in Ref. [56], $\tilde{h}_{\rm GR}$ is the GW waveform represented by IMRPhenomPv2 [54], and $u_2 \equiv (\pi\mathcal{M}f)^{1/3}$. In this investigation, we choose

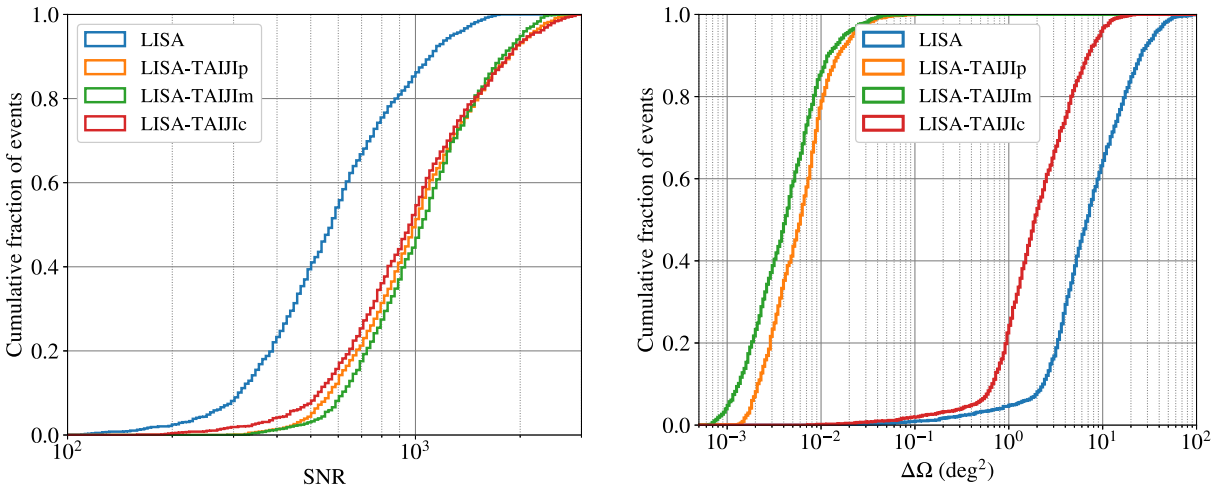

FIG. 3. The cumulative histograms of the SNR (left panel) and angular resolutions of the sky localization (right panel) from LISA and three LISA-TAIJI networks. All three LISA-TAIJI networks could achieve more than $\sqrt{2}$ times the SNR of the LISA mission alone. Of the three networks, the SNR from LISA-TAIJIm has the most concentrated distribution because it uses the most averaged antenna pattern, as shown in Fig. 2. The distribution of SNR from LISA-TAIJIc has a long tail, since the two missions share the same sensitive/insensitive areas. In the right plot, the resolution of the sky localization by LISA-TAIJIc is shown to be approximately twice that of LISA alone as the attribute to the SNR increase. The angular resolution of the LISA-TAIJIp is better than that of LISA-TAIJIc, benefiting from the long separation. Finally, the performance of LISA-TAIJIm is better than that of LISA-TAIJIp, because the angle between the LISA and TAIJIm formation planes is 71°, an orientation that can yield a more collaborative antenna pattern.

$b = -3$, which corresponds to the massive graviton theory [57–63], and we set $\beta = 0.01$, which is from the rough boundary constrained in Ref. [64]. The other four ppE parameters tuning the amplitudes of the alternative polarizations are set to zero: $(\alpha_b, \alpha_L, \alpha_x, \alpha_y) = (0, 0, 0, 0)$. Although this specific selection could not represent all other gravity theories, we have demonstrated that the measurement on the ppE parameters could also be similarly improved by the LISA-TAIJI network for other value choices [30].

The constraints on the ppE parameters α for the scalar (upper panel) and vector (lower panel) polarizations are shown in Fig. 4. Similar to the results achieved for the sky localization, the constraint on α from the LISA-TAIJIc configuration is more than $\sqrt{2}$ times better than that for LISA alone, which is an attribute from the increased SNR. The LISA-TAIJIp network, with its large separation, could improve the constraints on the polarizations significantly. And LISA-TAIJIm could achieve the best constraints on the polarizations of the three LISA-TAIJI configurations as the benefit of better antenna pattern cooperation.

IV. OVERLAP REDUCTION FUNCTION OF THE LISA-TAIJI NETWORKS

The response of the detector network to the stochastic background GW signal will depend on the locations and orientations of the interferometers. Flanagan [65] evaluated the sensitivities of the ground-based GW interferometers to the stochastic background. An *overlap reduction function* is introduced to indicate the cross-correlation between a

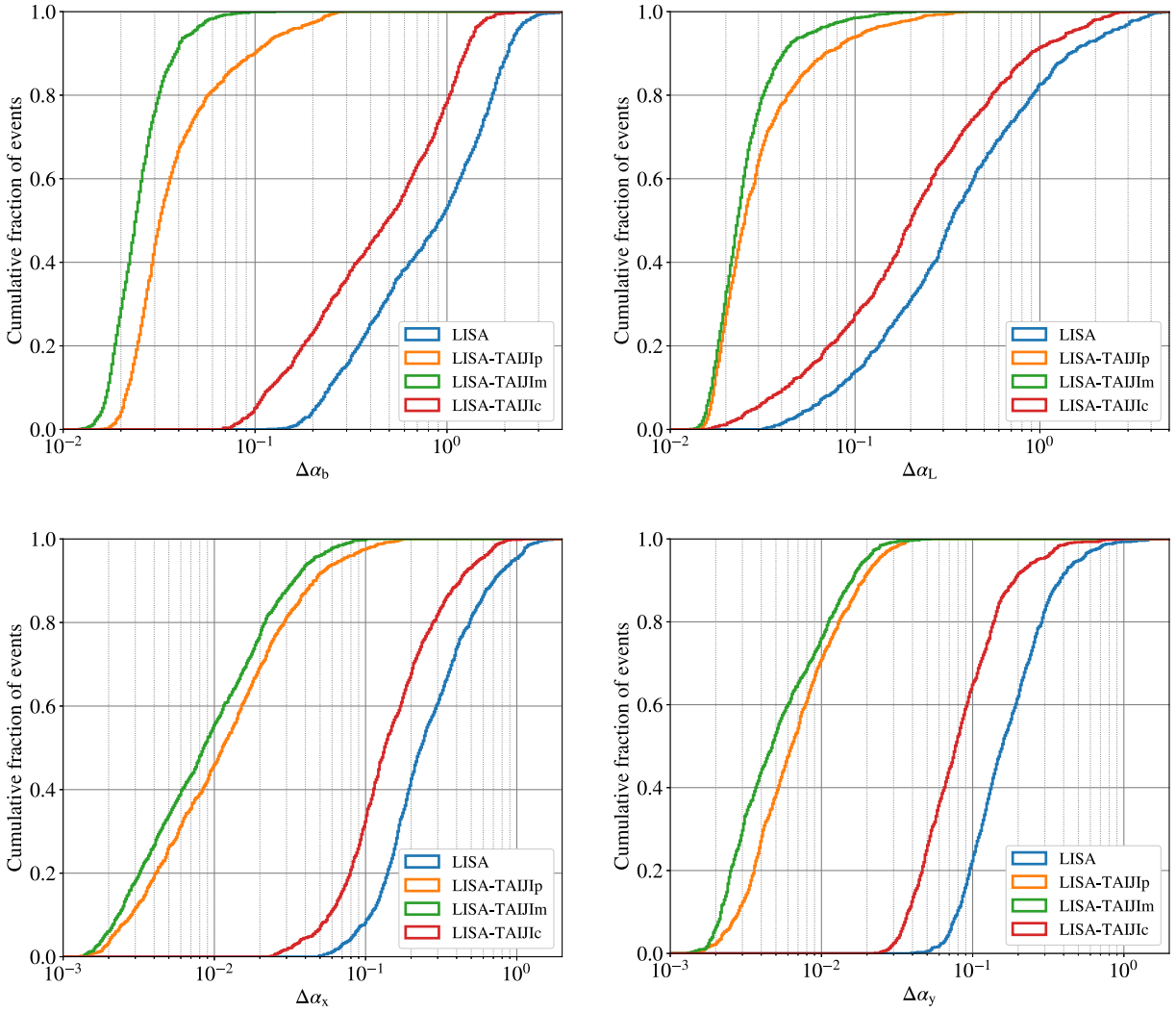

FIG. 4. The cumulative histograms of the constraints on the amplitudes of scalar and vector polarizations. The result from the LISA-TAIJIc configuration is more than $\sqrt{2}$ times better than that of LISA alone, which is an attribute from the increase of the SNR. The LISA-TAIJIp network, with its long baseline separation, could significantly improve the constraints on polarizations. And LISA-TAIJIm achieves the best constraints on the polarizations of the three LISA-TAIJI configurations as the benefit of better antenna pattern cooperation.

pair of detectors [66]. Whelan *et al.* [67] calculated the overlap reduction functions for the two LIGO detectors and GEO. Omiya and Seto [25], Seto [26], and Orlando *et al.* [27] specified the overlap function of the LISA-TAIJIp network for optimal TDI channels and alternative GW polarizations. Schmitz [17] reviewed the detectability of the ground- and space-based detectors for the stochastic GW background.

For a single LISA-like mission with a full six measurement links, the optimal TDI channels could be treated as three equivalent interferometers. The observations from these TDI channels could be used to discriminate the stochastic GW background from the instrument noise [68], and the motion of the detectors may also help to resolve the background, especially for the anisotropic signal [16]. LISA and TAIJI could form an ideal network to separate the cosmological SGWB signal from other stochastic processes such as the instrument noise and astrophysical foreground.

To characterize the cross-correlation between LISA and different TAIJI orbital configurations, their overlap reduction functions are calculated for different polarizations,

$$\gamma_{\mathrm{ab,p}}(f) = \frac{\kappa}{4\pi}\int \mathrm{d}\mathbf{n} \sum_{\mathrm{A,E,T}} F^{\mathrm{a}}_{\mathrm{TDI,p}}(f,\mathbf{n}) \sum_{\mathrm{A,E,T}} F^{\mathrm{b}}_{\mathrm{TDI,p}}(f,\mathbf{n}), \quad (19)$$

where $F^{\mathrm{a}}_{\mathrm{TDI,p}}$ is the response function to the polarization mode "p" (tensor, vector, scalar breathing, and scalar longitudinal) in the TDI channel from the mission "a," and κ is the normalization factor to make $\gamma_{\mathrm{ab}} = 1$ when the two detectors are coaligned and colocalized. The polarization angle ψ is set to zero, and the inclination ι is set to be optimal for each polarization mode.

The overlap reduction functions for the different LISA-TAIJI networks for different polarizations are shown in Fig. 5. Since the orientations of LISA and TAIJIc are aligned, and since they are coplanar and at the same

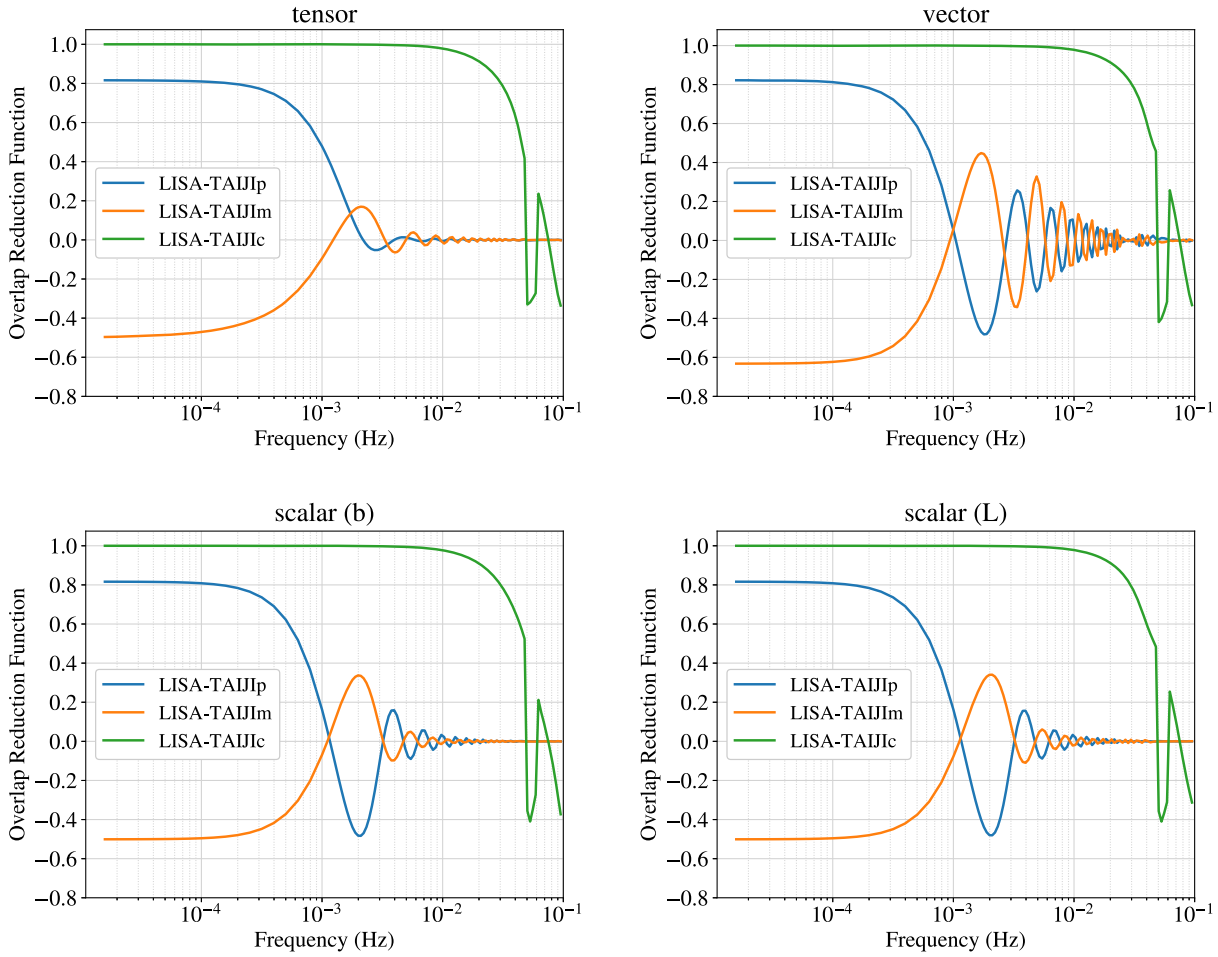

FIG. 5. The overlap reduction functions of three LISA-TAIJI networks for different polarization modes. The overlap function of the LISA-TAIJIc network is unity for frequencies lower than 10 mHz, which is optimal for SGWB observation, and it changes sign during the two detectors' characteristic frequencies gap [50 mHz, 60 mHz]. The overlap functions of the LISA-TAIJIp and LISA-TAIJIm networks are close to zero around 1.5 mHz due to their 1×10^8 km separations [$f_{\mathrm{crit}} = c/(2 \times 1 \times 10^8\ \mathrm{km}) \simeq 1.5$ mHz]. The LISA-TAIJIm network has a worse cross-correlation than the LISA-TAIJIp because of its more misaligned orientation.

location, the overlap function of the LISA-TAIJIc network is unity for frequencies lower than 10 mHz, which indicates the strong correlation between the LISA and TAIJIc detectors, and the network is optimal for SGWB observation for all polarization modes. We also notice that their overlap reduction functions change sign during the two detectors' characteristic frequencies gap [$\frac{c}{2L_{\mathrm{TAIJI}}} = 50$ mHz, $\frac{c}{2L_{\mathrm{LISA}}} = 60$ mHz] (c is the speed of light in this section).

Considering the 1×10^8 km separation between LISA and TAIJIp/TAIJIm, we can see the overlap reduction functions quickly approach zero around a critical frequency $f_{\mathrm{crit}} \simeq c/(2 \times 1 \times 10^8\ \mathrm{km}) \simeq 1.5$ mHz [16], and they oscillate and decay with increasing frequency. The γ_{ab} from the LISA-TAIJIp pair is higher than the value from LISA-TAIJIm because the orientation of LISA is more aligned with TAIIJIp (34.5°) than with TAIJIm (71°), which causes TAIJIp to have a stronger correlation with LISA. Therefore, of the three LISA-TAIJI networks, LISA-TAIJIm should be the relatively worst configuration for SGWB detection.

There will be a tradeoff for a LISA-like GW detector network to observe compact binary systems and the SGWB. A long baseline for detector deployment will promote the accuracy of parameter estimation for SMBH binaries. However, the frequency for the detectable SGWB band would be lowered, referring to the critical frequency:

$$f_{\mathrm{crit}} = \frac{c}{2d} = \frac{c}{2 \times 2\ \mathrm{AU} \sin\frac{\epsilon}{2}} \simeq \frac{0.5\ \mathrm{mHz}}{\sin\frac{\epsilon}{2}}, \qquad (20)$$

where d is the distance between two detectors, and ϵ is the separation angle formed by the two lines connecting the Sun and the detectors.

On the other hand, the angle between the constellation planes also changes with the separation angle, as shown in Fig. 6. Considering the orientation of the plane with an angle close to 90° should be helpful to resolve the source parameters; the composition of a +60° with a −60° inclination could be more cooperative than the two missions with the same inclination for a separation angle smaller than 90°. For the BBO or DECIGO missions, the constellations are planned to be separated by 120°, and two options could be considered for their orientation deployment—83° or 51° with respect to another formation plane, as tagged in Fig. 6.

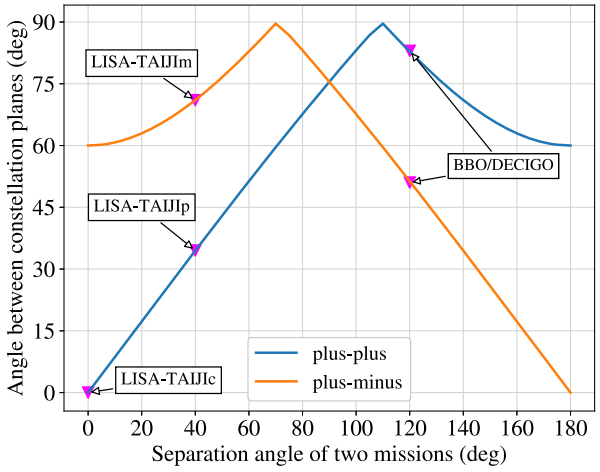

FIG. 6. The angle of the formation planes varying with the separation angle of two constellations of spacecraft. The "plus-plus" curve indicates the two constellations having +60° inclinations with respect to the ecliptic plane, and the "plus-minus" curve indicates one constellation having a +60° inclination and the other having a −60° inclination.

V. CONCLUSIONS

In this work, we investigate the performances of three alternative LISA-TAIJI networks on the sky localizations and polarization observations of SMBH binaries and the overlap reduction function for the stochastic gravitational wave background observation. For SMBH binary systems, compared to the LISA mission alone, the colocated and coplanar LISA-TAIJIc network ordinarily improves the SNR and parameter resolution by a factor of $\sqrt{2}$. With a 1×10^8 km separation, the joint observations from LISA and TAIJIp significantly improve parameter determinations for SMBH binaries over the LISA-TAIJIc configuration. The LISA-TAIJIm network demonstrates a better capability to determine the sky location and polarizations than the LISA-TAIJIp network as benefits of its more misaligned orientation and complementary antenna pattern. For the detectability of the stochastic gravitational wave background, the LISA-TAIJIc network would have optimal performance as a benefit of its coplanar formation and colocation, while the LISA-TAIJIm network would present the worst cross-correlation with the LISA due to the fact that it is the orientation least aligned with LISA among the three TAIJI orbital configurations.

One lesson from this evaluation of three LISA-TAIJI networks is that the parameter resolution of the compact binary coalescences will be impacted by the SNR, the distance of detector separation, and the cooperative orientations of the detectors. Both of the next-generation space-based GW detectors, DECIGO and BBO, are proposed to use a LISA-like orbit with multiple constellations to detect the relic GWs left by the big bang, intermediate-mass black holes, etc., in the deci-Hz frequency band [14,15]. The parameter resolution improvements have been performed for the compact binaries in Ref. [14] as the results of multiple interferometers and long baselines. The orientation combinations of the constellations are also worth evaluating for the targeting sources.

Beyond the LISA-like orbital formation, various space missions are proposed to arrange spacecraft equally on a planetary orbit in order to observe GWs in the micro-Hz band—for instance, ASTROD-GW [69], the Folkner mission [70], and μAres [71], etc. ASTROD-GW is initially proposed to deploy three spacecraft around Lagrange points L3, L4, and L5 of the Sun-Earth system, and an

extended deployment could use six spacecraft to form two triangular interferometers to enhance the sensitivity to the SGWB [69]. μAres will place two orthogonal triangle interferometers with respect to the Mars (or Earth/Venus) orbit. The tradeoff of detectability from various deployments could also be explored to balance the GW observations from compact binary systems and the cosmological stochastic background.

ACKNOWLEDGMENTS

This work was supported by NSFC Grants No. 12003059 and No. 11773059, and the Strategic Priority Research Program of the Chinese Academy of Sciences under Grant No. XDA15021102. This work made use of the High Performance Computing Resource in the Core Facility for Advanced Research Computing at Shanghai Astronomical Observatory.

[1] B. P. Abbott *et al.* (LIGO Scientific, Virgo Collaborations), Observation of Gravitational Waves from a Binary Black Hole Merger, Phys. Rev. Lett. **116**, 061102 (2016).
[2] B. P. Abbott *et al.* (LIGO Scientific, Virgo Collaborations), GW170814: A Three-Detector Observation of Gravitational Waves from a Binary Black Hole Coalescence, Phys. Rev. Lett. **119**, 141101 (2017).
[3] B. P. Abbott *et al.* (LIGO Scientific, Virgo Collaborations), GW170817: Observation of Gravitational Waves from a Binary Neutron Star Inspiral, Phys. Rev. Lett. **119**, 161101 (2017).
[4] B. P. Abbott *et al.* (LIGO Scientific, Virgo Collaborations), Tests of General Relativity with GW170817, Phys. Rev. Lett. **123**, 011102 (2019).
[5] T. Akutsu *et al.* (KAGRA Collaboration), Overview of KAGRA: KAGRA science, Prog. Theor. Exp. Phys. **2021**, 05A103 (2021).
[6] B. P. Abbott *et al.* (KAGRA, LIGO Scientific, Virgo Collaborations), Prospects for observing and localizing gravitational-wave transients with Advanced LIGO, Advanced Virgo and KAGRA, Living Rev. Relativity **23**, 3 (2020).
[7] B. F. Schutz, Networks of gravitational wave detectors and three figures of merit, Classical Quantum Gravity **28**, 125023 (2011).
[8] B. P. Abbott *et al.* (LIGO Scientific, Virgo Collaborations), Upper Limits on the Stochastic Gravitational-Wave Background from Advanced LIGO's First Observing Run, Phys. Rev. Lett. **118**, 121101 (2017); **119**, 029901(E) (2017).
[9] B. P. Abbott *et al.* (LIGO Scientific, Virgo Collaborations), Search for Tensor, Vector, and Scalar Polarizations in the Stochastic Gravitational-Wave Background, Phys. Rev. Lett. **120**, 201102 (2018).
[10] B. P. Abbott *et al.* (LIGO Scientific, Virgo Collaborations), Search for the isotropic stochastic background using data from Advanced LIGO's second observing run, Phys. Rev. D **100**, 061101 (2019).
[11] R. Abbott *et al.* (LIGO Scientific, Virgo, KAGRA Collaborations), Upper limits on the isotropic gravitational-wave background from Advanced LIGO's and Advanced Virgo's third observing run, arXiv:2101.12130.
[12] R. Abbott *et al.* (LIGO Scientific, Virgo, KAGRA Collaborations), Constraints on cosmic strings using data from the third Advanced LIGO-Virgo observing run, arXiv:2101.12248.
[13] R. Abbott *et al.* (LIGO Scientific, Virgo, KAGRA Collaborations), Search for anisotropic gravitational-wave backgrounds using data from Advanced LIGO's and Advanced Virgo's first three observing runs, arXiv:2103.08520.
[14] J. Crowder and N. J. Cornish, Beyond LISA: Exploring future gravitational wave missions, Phys. Rev. D **72**, 083005 (2005).
[15] S. Kawamura *et al.*, The Japanese space gravitational wave antenna DECIGO, Classical Quantum Gravity **23**, S125 (2006).
[16] J. D. Romano and N. J. Cornish, Detection methods for stochastic gravitational-wave backgrounds: A unified treatment, Living Rev. Relativity **20**, 2 (2017).
[17] K. Schmitz, New sensitivity curves for gravitational-wave signals from cosmological phase transitions, J. High Energy Phys. 01 (2021) 097.
[18] W.-T. Ni, Mid-frequency gravitational wave detection and sources, Int. J. Mod. Phys. D **29**, 1902005 (2020).
[19] P. Amaro-Seoane, H. Audley, S. Babak *et al.* (LISA Team Collaborations), Laser interferometer space antenna, arXiv:1702.00786.
[20] W.-R. Hu and Y.-L. Wu, The Taiji Program in Space for gravitational wave physics and the nature of gravity, Natl. Sci. Rev. **4**, 685 (2017).
[21] J. Luo *et al.* (TianQin Team Collaborations), TianQin: A space-borne gravitational wave detector, Classical Quantum Gravity **33**, 035010 (2016).
[22] S. V. Dhurandhar, K. Rajesh Nayak, S. Koshti, and J. Y. Vinet, Fundamentals of the LISA stable flight formation, Classical Quantum Gravity **22**, 481 (2005).
[23] W.-H. Ruan, C. Liu, Z.-K. Guo, Y.-L. Wu, and R.-G. Cai, The LISA-Taiji network, Nat. Astron. **4**, 108 (2020).
[24] G. Wang, W.-T. Ni, W.-B. Han, S.-C. Yang, and X.-Y. Zhong, Numerical simulation of sky localization for LISA-TAIJI joint observation, Phys. Rev. D **102**, 024089 (2020).
[25] H. Omiya and N. Seto, Searching for anomalous polarization modes of the stochastic gravitational wave background with LISA and Taiji, Phys. Rev. D **102**, 084053 (2020).
[26] N. Seto, Gravitational wave background search by correlating multiple triangular detectors in the mHz band, Phys. Rev. D **102**, 123547 (2020).

[27] G. Orlando, M. Pieroni, and A. Ricciardone, Measuring parity violation in the stochastic gravitational wave background with the LISA-Taiji network, J. Cosmol. Astropart. Phys. 03 (2021) 069.
[28] R. Wang, W.-H. Ruan, Q. Yang, Z.-K. Guo, R.-G. Cai, and B. Hu, Hubble parameter estimation via dark sirens with the LISA-Taiji network, arXiv:2010.14732.
[29] L.-F. Wang, S.-J. Jin, J.-F. Zhang, and X. Zhang, Forecast for cosmological parameter estimation with gravitational-wave standard sirens from the LISA-Taiji network, arXiv:2101.11882.
[30] G. Wang and W.-B. Han, Observing gravitational wave polarizations with the LISA-TAIJI network, Phys. Rev. D **103**, 064021 (2021).
[31] LISA Study Team, LISA (Laser Interferometer Space Antenna): A Cornerstone Mission for the Observation of Gravitational Waves, Technical Report No. 11, ESA-SCI, 2000, System and Technology Study Report.
[32] G. Wang and W.-T. Ni, Numerical simulation of time delay interferometry for TAIJI and new LISA, Res. Astron. Astrophys. **19**, 058 (2019).
[33] G. Wang and W.-T. Ni, Time-delay interferometry for ASTROD-GW, Chin. Astron. Astrophys. **36**, 211 (2012), and references therein.
[34] G. Wang and W.-T. Ni, Numermcal simulation of time delay interferometry for NGO/eLISA, Classical Quantum Gravity **30**, 065011 (2013).
[35] G. Wang and W.-T. Ni, Orbit optimization for ASTROD-GW and its time delay interferometry with two arms using CGC ephemeris, Chin. Phys. B **22**, 049501 (2013).
[36] S. V. Dhurandhar, W. T. Ni, and G. Wang, Numerical simulation of time delay interferometry for a LISA-like mission with the simplification of having only one interferometer, Adv. Space Res. **51**, 198 (2013).
[37] G. Wang and W.-T. Ni, Orbit optimization and time delay interferometry for inclined ASTROD-GW formation with half-year precession-period, Chin. Phys. B **24**, 059501 (2015).
[38] G. Wang, W.-T. Ni, and W.-B. Han, Revisiting time delay interferometry for unequal-arm LISA and TAIJI, arXiv:2008.05812.
[39] G. Wang, W.-T. Ni, W.-B. Han, and C.-F. Qiao, Algorithm for TDI numerical simulation and sensitivity investigation, Phys. Rev. D **103**, 122006 (2021).
[40] F. B. Estabrook and H. D. Wahlquist, Response of Doppler spacecraft tracking to gravitational radiation, Gen. Relativ. Gravit. **6**, 439 (1975).
[41] H. Wahlquist, The Doppler response to gravitational waves from a binary star source, Gen. Relativ. Gravit. **19**, 1101 (1987).
[42] M. Vallisneri, J. Crowder, and M. Tinto, Sensitivity and parameter-estimation precision for alternate LISA configurations, Classical Quantum Gravity **25**, 065005 (2008).
[43] M. Vallisneri and C. R. Galley, Non-sky-averaged sensitivity curves for space-based gravitational-wave observatories, Classical Quantum Gravity **29**, 124015 (2012).
[44] M. Tinto and M. E. da Silva Alves, LISA sensitivities to gravitational waves from relativistic metric theories of gravity, Phys. Rev. D **82**, 122003 (2010).
[45] T. A. Prince, M. Tinto, S. L. Larson, and J. W. Armstrong, The LISA optimal sensitivity, Phys. Rev. D **66**, 122002 (2002).
[46] M. Otto, G. Heinzel, and K. Danzmann, TDI and clock noise removal for the split interferometry configuration of LISA, Classical Quantum Gravity **29**, 205003 (2012).
[47] M. Otto, Ph.D. thesis, Leibniz Universität, Hannover, 2015.
[48] M. Tinto and O. Hartwig, Time-delay interferometry and clock-noise calibration, Phys. Rev. D **98**, 042003 (2018).
[49] Z. Luo, Z. Guo, G. Jin, Y. Wu, and W. Hu, A brief analysis to Taiji: Science and technology, Results Phys. **16**, 102918 (2020).
[50] C. Cutler and É. E. Flanagan, Gravitational waves from merging compact binaries: How accurately can one extract the binary's parameters from the inspiral waveform?, Phys. Rev. D **49**, 2658 (1994).
[51] C. Cutler, Angular resolution of the LISA gravitational wave detector, Phys. Rev. D **57**, 7089 (1998).
[52] M. Vallisneri, Use and abuse of the Fisher information matrix in the assessment of gravitational-wave parameter-estimation prospects, Phys. Rev. D **77**, 042001 (2008).
[53] K. A. Kuns, H. Yu, Y. Chen, and R. X. Adhikari, Astrophysics and cosmology with a deci-Hertz gravitational-wave detector: TianGO, Phys. Rev. D **102**, 043001 (2020).
[54] S. Khan, S. Husa, M. Hannam, F. Ohme, M. Pürrer, X. J. Forteza, and A. Bohé, Frequency-domain gravitational waves from nonprecessing black-hole binaries: II. A phenomenological model for the advanced detector era, Phys. Rev. D **93**, 044007 (2016).
[55] K. Chatziioannou, N. Yunes, and N. Cornish, Model-independent test of general relativity: An extended post-Einsteinian framework with complete polarization content, Phys. Rev. D **86**, 022004 (2012).
[56] K. Chatziioannou, N. Yunes, and N. Cornish, Model-independent test of general relativity: An extended post-Einsteinian framework with complete polarization content Phys. Rev. D **86**, 022004 (2012).**95**, 129901(E) (2017).
[57] C. M. Will, Bounding the mass of the graviton using gravitational wave observations of inspiralling compact binaries, Phys. Rev. D **57**, 2061 (1998).
[58] C. M. Will and N. Yunes, Testing alternative theories of gravity using LISA, Classical Quantum Gravity **21**, 4367 (2004).
[59] E. Berti, A. Buonanno, and C. M. Will, Testing general relativity and probing the merger history of massive black holes with LISA, Classical Quantum Gravity **22**, S943 (2005).
[60] A. Stavridis and C. M. Will, Bounding the mass of the graviton with gravitational waves: Effect of spin precessions in massive black hole binaries, Phys. Rev. D **80**, 044002 (2009).
[61] K. G. Arun and C. M. Will, Bounding the mass of the graviton with gravitational waves: Effect of higher harmonics in gravitational waveform templates, Classical Quantum Gravity **26**, 155002 (2009).
[62] D. Keppel and P. Ajith, Constraining the mass of the graviton using coalescing black-hole binaries, Phys. Rev. D **82**, 122001 (2010).

[63] K. Yagi and T. Tanaka, Constraining alternative theories of gravity by gravitational waves from precessing eccentric compact binaries with LISA, Phys. Rev. D **81**, 064008 (2010); **81**, 109902(E) (2010).

[64] N. Cornish, L. Sampson, N. Yunes, and F. Pretorius, Gravitational wave tests of general relativity with the parameterized post-Einsteinian framework, Phys. Rev. D **84**, 062003 (2011).

[65] E. E. Flanagan, The sensitivity of the laser interferometer gravitational wave observatory (LIGO) to a stochastic background, and its dependence on the detector orientations, Phys. Rev. D **48**, 2389 (1993).

[66] N. Christensen, Measuring the stochastic gravitational radiation background with laser interferometric antennas, Phys. Rev. D **46**, 5250 (1992).

[67] J. T. Whelan, W. G. Anderson, M. Casquette, M. C. Diaz, I. S. Heng, M. McHugh, J. D. Romano, C. W. Torres, Jr., R. M. Trejo, and A. Vecchio, Progress on stochastic background search codes for LIGO, Classical Quantum Gravity **19**, 1521 (2002).

[68] M. R. Adams and N. J. Cornish, Discriminating between a stochastic gravitational wave background and instrument noise, Phys. Rev. D **82**, 022002 (2010).

[69] W.-T. Ni, ASTROD-GW: Overview and progress, Int. J. Mod. Phys. D **22**, 1341004 (2013).

[70] J. Baker *et al.*, Space Based Gravitational Wave Astronomy Beyond LISA, arXiv:1907.11305.

[71] A. Sesana *et al.*, Unveiling the gravitational Universe at μ-Hz frequencies, arXiv:1908.11391.